Identification of the in vivo elastic properties of common carotid arteries from MRI: a study on subjects with and without atherosclerosis.

Alexandre Franquet, Stéphane Avril, Rodolphe Le Riche, Pierre Badel, Fabien Schneider, Chrisitan Boissier, Jean-Pierre Favre

Identification of the *in vivo* elastic properties of common carotid arteries from MRI: a study on subjects with and without atherosclerosis.

A. Franquet[1], S. Avril[1], R. Le Riche[2], P. Badel[1], F.C. Schneider[3], C. Boissier[4], J-P. Favre[5]

1 CIS-EMSE, CNRS UMR 5146, Ecole Nationale Supérieure des Mines, Saint-Etienne F-42023,France

2 CNRS UMR 6158 and H. Fayol Institute, Ecole Nationale Supérieure des Mines, Saint-Etienne F-42023,France

3 Radiology Department, University Hospital, GRT-PAR UR4672, Université Jean Monnet, Saint-Etienne F-42023, France

4 Vascular Medicine Department, University Hospital, GRT-PAR UR4672, Université Jean Monnet, Saint-Etienne F-42023, France

5 Cardiovascular Surgery Department, University Hospital, GRT-PAR UR4672, Université Jean Monnet, Saint-Etienne F-42023, France

Abstract

The stiffness of the arterial wall, which is modified by many cardiovascular diseases such as atherosclerosis, is known to be an indicator of vulnerability. This work focuses on the *in vivo* quantification of the stiffness of the common carotid artery (CCA) by applying the Magnitude Based Finite Element Model Updating (MB-FEMU) method to 13 healthy and diseased volunteers aged from 24 to 76 years old. The MB-FEMU method is based on the minimisation of the deviation between the image of a deformed artery and a registered image of this artery deformed by means of a finite elements analysis. Cross sections of the neck of each subject at different times of the cardiac cycle are

recorded using a Phase Contrast cine-MRI. Applanation tonometry is then performed to obtain the blood pressure variations in the CCA throughout a heart beat. First, a time averaged elastic modulus of each CCA between diastole and systole is identified and a stiffening of the artery with age and disease is observed. Second, four elastic moduli are identified during a single heart beat for each artery, highlighting the nonlinear mechanical behaviour of the artery. A stiffening of the artery is observed and quantified at systole in comparison to diastole.

Keywords

Identification, mechanical properties, elasticity, finite elements analysis, *in vivo* analysis, MRI, artery

1 Introduction

Arterial stiffness is known to be a crucial indicator for the diagnosis of arterial health [14]. This indicator provides information on the ageing of the artery, or on the progress of diseases such as atherosclerosis [19, 37] which mainly concerns the coronary and the carotid arteries. Identifying the elastic properties of the Common Carotid Artery (CCA) of a patient could then be a tool for improving diagnoses.

A variety of noninvasive techniques have been developed and used to try to identify the arterial stiffness *in vivo*. The Pulse Wave Velocity for instance is an indicator of the mean arterial stiffness. It is estimated by measuring the travel time of a wave between two measurement sites [33]. More advanced methods are used for the local assessment of the arterial stiffness. Many studies track the change of arterial diameter during heart beat by ultrasounds [30, 21, 4, 6, 3, 2]. The blood pressure is generally measured in parallel on the brachial artery. The elastic modulus is then deduced from these measurements by using assumptions such as the perfect circularity of the artery with a free outer contour. For instance [30] have shown that the elastic modulus of the CCA tends to increase with age. If this kind of approaches has the advantage to be simple, and can be used for a rapid examination, the complex nonlinear mechanical behaviour of arteries [11, 13, 28] cannot be assessed by a unique

modulus without requiring the linearisation of the stress-strain curve. To this aim, other studies have considered nonlinearities and identified either nonlinear [25, 23] or multi-linear [8, 15, 16] constitutive properties of the artery. Eventhough the artery is still simplified as a tube, these recent studies have incorporated a surrounding tissue around the artery. It has been shown that the surrounding tissue plays an important role in the strain which effectively occurs in the artery (and as a consequence, on the stresses) and then must be included in the models for the identification of the mechanical properties [38, 24, 22, 27, 10]. Similarly the measurement of the blood pressure is a sensitive step since it is directly involved in the estimation of the elastic properties [17, 10]. A new methodology for identifying the mechanical properties of tissues from MRI has recently been designed in our team [10]: the Magnitude Based Finite Element Model Updating Method (MB-FEMU) works by registering a template image using a Finite Element Analysis. The registered image, which depends on the elastic properties input to the FE model, is compared to a target image. The identification of the elastic properties of the FE model consists in minimising the difference between the target and the registered image by iteratively updating the elastic properties. The template and the target images are two experimental images obtained using a cine Magnetic Resonance Imaging (MRI) sequence at different times of the cardiac cycle.

In the current work, we investigate the identification of the elastic modulus of the CCA *invivo* using the MB-FEMU method. It has been applied in clinical conditions to 9 healthy volunteers (24 to 63 years old) and 4 volunteer patients with atherosclerosis (68 to 76 years old). A unique elastic modulus is first considered before studying the evolution of the elastic modulus through the cardiac cycle. The influence of the surrounding tissue and of the measurement of the blood pressure on the identified mechanical properties is discussed in details.

2 Methods

2.1 Subjects and patients

The following research protocol was approved by the review board of Saint-Etienne University Hospital and informed consent was obtained from all subjects. The subjects studied were separated into three groups. The first group was named the "Young healthy subjects" and was composed of 4 men without any declared disease aged from 24 to 26 years old. The second group of subjects (dubbed "Mid-age healthy subjects") was made of 5 healthy subjects (1 woman and 4 men) aged from 51 to 63 years old. The third group, named "Old diseased patients" was composed of 3 men with severe (>80% diameter reduction) unilateral carotid bifurcation occlusive disease and 1 woman with a bilateral post-radiation stenosis (>80%) aged from 68 to 76 years (report to the Table 1).

The mechanical properties of the CCA were estimated from Magnetic Resonance 2D images. A dedicated (1^{st} and 2^{nd} groups) or additional (3^{rd} group) Phase Contrast (PC) sequence was used to obtain slices of the neck at different times of the cardiac cycle (cine MRI). The acquisition of PC images lasts approximately 5 minutes depending on the heart rate of each individual. The subjects spent a total time of approximately 30 minutes in the MRI (including 3 slices of the arterial tree in cine MRI, positioning MR sequences -Time Of Flight-, Turbo Spin Echo sequences -T1 and T2 weighted images-). In this study only the PC cine MRI of one slice of the CCA was used. The patients spent 45 minutes in the device including the additional sequence and the routine pre-surgical cerebral sequence.

15 minutes after the MRI the subjects and patients had an applanation tonometry examination in order to measure the variation of their blood pressure during a cardiac cycle (a probe is applied on the carotid artery by a trained physician to derive the physiological signal). Blood pressure was also measured before and after the MRI (and during the MRI for 2 healthy subjects). For all the healthy subjects, an additional echography was performed in order to measure the Intima-Media Thickness of their common carotid. The experimental protocol is summarised in Figure 1.

Table 1: Description of the subjects. Three groups were defined: the "Young Healthy subjects" (YH) group, the "Mid Age Healthy subjects" (MAH) group and the "Old Diseased patients" (OD) group. IMT is the Intima Media Thickness which was measured by ultrasounds except for the OD group where values from the literature were used [7].

Subject Patient	Gender	Age (years)	Height (cm)	Weight (kg)	Diseased artery	IMT left/right (mm)
YH1	M	25	185	85	No	0.45/0.45
YH2	M	24	183	80	No	0.43/0.43
YH3	M	25	182	85	No	0.45/0.45
YH4	M	26	180	70	No	0.44/0.44
MAH1	M	59	163	72	No	0.83/0.72
MAH2	M	63	179	72	No	0.56/0.49
MAH3	M	51	175	74	No	0.62/0.51
MAH4	M	53	165	65	No	0.56/0.47
MAH5	F	57	155	62	No	0.58/0.48
OD1	F	70	158	57	Left/Right	0.70/0.70
OD2	M	68	182	87	Right	0.73/0.73
OD3	M	75	170	82	Right	0.73/0.73
OD4	M	76	178	78	Right	0.73/0.73

2.2 Imaging modalities

Magnetic Resonance Imaging was used with a Phase Contrast sequence to provide the cross section of the carotid artery at different time steps (cine MRI). A 3T Siemens Verio combined with a 4-Channel flex coil was used with a 2D spin echo FLASH sequence to provide series of images during the cardiac cycle. The acquisition of images was synchronised with the physiological signal which was captured by an infrared spectroscopy device fixed on the subject's finger. A single 4 mm thick slice was used. The 2D in plane resolution was $0.586\ \text{mm} \times 0.586\ \text{mm}$. The slice's position was 27 mm below the carotid bifurcation which was located on Time Of Flight images. Its orientation was chosen to cut the two common carotid arteries perpendicularly. The acquisition frequency was set automatically for each subject depending on his or her heart rate, providing between 35 and 50 images per cardiac cycle. Note that these

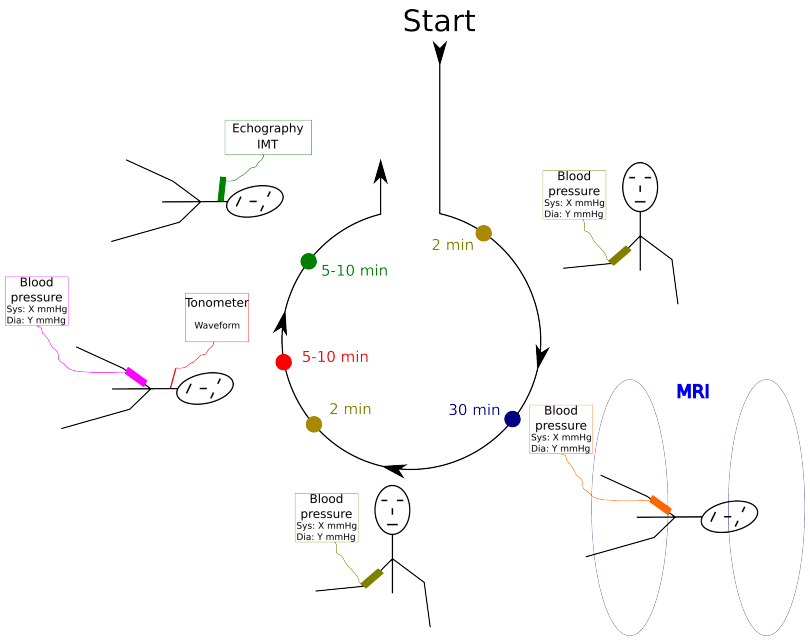

Figure 1: Description of the experimental protocol for a healthy subject. After admission at the radiological service, the blood pressure is measured by a trained physician using a digital sphygmomanometer. The MR exam lasts approximately 30 minutes depending in part on the heart rate of each subject. Note that the diseased patients spend 15 more minutes in the tube for their routine pre-surgical MR exam. The blood pressure is then measured in the radiological service one more time. The subjects reach the service of vascular medicine and after few minutes of rest, have an applanation tonometry examination with a trained physician where their blood pressure is recorded in order to scale their wave form obtained by tonometry. Finally, for the healthy subjects, it was possible to perform an echography in order to measure the Intima Media Thickness.

images were reconstructed from several cardiac cycles although an image sample at each time step was recorded at each cardiac cycle. The magnitude of images was digitised with a 12 bits resolution so that each voxel has an integer value between 0 and $4,095$.

For each subject and each artery, a region of interest of 21×21 pixels centred on the carotid was delineated on the magnitude PC images which yields the raw 2D experimental images recorded at different time steps. The images were filtered

along the time axis using a temporal Gaussian filter with a kernel size $\sigma = 1.5$. Each carotid was considered as independent so that the total number of experiments reached $2 \times 13 = 26$ specimens.

2.3 Identification method

The Magnitude-Based Finite Element Model Updating method (MB-FEMU), which has some common features with the Modality Independent Elastography method [36], was developed in a previous work [10]. The principle is to build up a registered image from an initial, measured, template image using a displacement field computed by a Finite Element Analysis. The elastic properties of the finite elements model are updated until the registered image matches a target measured image. The template and the target images correspond to the initial undeformed and deformed (i.e. after the application of external forces) states, respectively. In our case, the imaged object was a cross section of the CCA, and the force applied between the template and the target was the differential blood pressure. This technique requires the acquisition of both the images of the artery at two different times of the cardiac cycle, and the differential blood pressure between these two times. Note also that a correction of rigid motions between the template and the target images was applied before the use of the MB-FEMU (see Section 2.5.2). The flow-chart of the method is summarised in Figure 2.

The identification of the mechanical properties was achieved by minimising a cost function defined as the difference in intensity between the target image and the registered image:

$$J_2(E) = \frac{1}{2 \cdot N_{pix}} \sum_{i=1}^{N_{pix}} \left(I^i_{target} - I^i_{registered}(E) \right)^2 \tag{1}$$

This cost function was calculated only at the pixels where the partial volume effect occurs: the pixels are filled with different materials so their intensity values depend on the proportion of the different materials. A binary mask was defined to this aim, as the dilation of a first binary mask which contains the pixels where the inner contour of the artery was found (see Section 2.4.1). The first binary mask

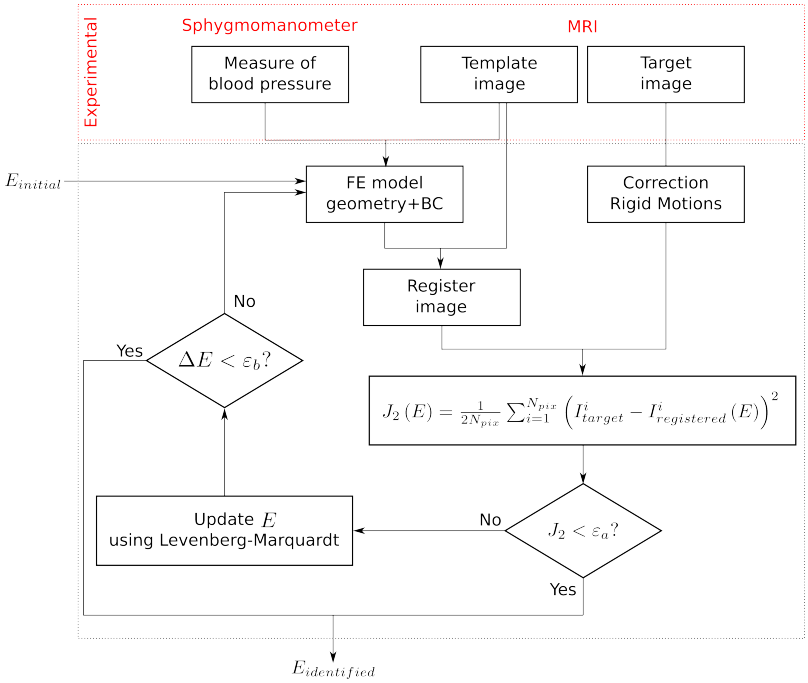

Figure 2: Flow-chart of the MB-FEMU method applied to the identification of the mechanical properties of the artery using MR images. A template and a target images are acquired using a MRI device. Blood pressure is measured at the same time. A finite element model is defined from the template image, mechanical assumptions, and blood pressure. The computed displacement field is a function of the elastic properties of the materials and is used to register the template image. Note that a procedure of correction of the rigid motions between the template and the target image is applied (see Section 2.5.2). A distance, J_2, between the registered image and the target image is minimised with regards to the elastic properties of the artery, E.

was dilated using a square structuring element S of size 3×3 with $S_{ij} = 1$ (see Figure 3). In our study we used a bounded Levenberg-Marquardt algorithm [12] to minimise the cost function. The gradients of the computed intensity with regards to the mechanical properties were calculated by backward finite differences. The identification algorithm stops when one of the following criteria was reached: either the target and the registered images matched well, $J_2 < \varepsilon_a = 1$, or the identification algorithm was making too small steps, $\Delta E < \varepsilon_b = 10^{-3}$.

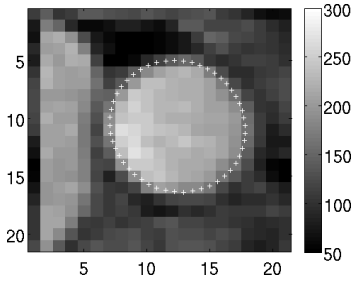

(a) Example of a template image from which the inner contour of the artery (white) was extracted (see Section 2.4.1).

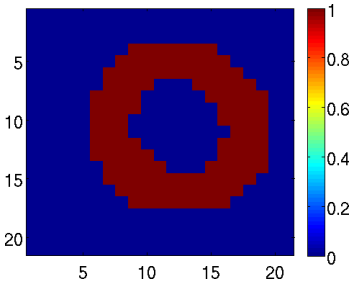

(b) Binary mask defined for this example.

Figure 3: Example of the definition of a binary mask on a template image. The cost function was only calculated where the binary mask is not null. The details of how the contour was obtained are described in Section 2.4.1.

2.4 Finite elements models and mechanical assumptions

2.4.1 FE model: geometry, boundary conditions and mesh definition

The geometry of the 2D FE models was derived from the initial (diastole) PC MR images of each subject. Each carotid was considered as independent so that two FE models were defined by subject, each representing a semi-neck. Three materials were segmented: (i) the inner contour of the carotid was determined by an automatic algorithm based on a Fourier polynomial description (see [10] for details). The artery was then defined as an homogeneous media and derived from this contour outwards with a thickness measured on an ultrasonic device (Intima Media Thickness (IMT) on the distal wall of each carotid artery). For the third experimental group ("old diseased group"), the IMT was not measured for non-medical reasons so thicknesses found in the literature [7] were used (0.70 mm for the woman and 0.73 mm for the men). (ii) An homogeneous material which surrounds the artery was segmented manually on the same initial image. The contours defined followed firstly, the jugular vein, secondly the external contour of the neck, and finally the spine. (iii) An artificial third material was created around the surrounding tissue. It had no mechanical influence and was only used for an easy implementation of our registration algorithm. Note that the radiological convention was applied throughout the manuscript. It means

that the left artery is located at the right of the spine and *vice versa*. The differences between the left and right geometries will be discussed in the Discussion section.

For the boundary conditions, the spine was fixed and a vertical symmetry was assumed since the semi-neck only was modelled for each experiment. A uniform pressure was applied on the inner arterial wall. It corresponds to the differential blood pressure measured on each subject between the deformed and the undeformed states.

The mesh consisted in approximately $8,000$ quadratic triangles (6 nodes) for each FE model. This type of element can provide accurate displacement fields for those types of problems [9]. The element size was refined on the artery's contour and close to it. Finally the artery had approximately $1,000$ elements and the surrounding tissue approximately $7,000$. The third "artificial" material had a coarse mesh (approximately 100 elements).

The FE computation ran on the 6.8 version of Abaqus© standard and took approximately 5 seconds on a desktop PC (Core Quad 2.5 GHz, 4 GB RAM).

2.4.2 Mechanical assumptions

As a first approximation the three materials were considered as linear elastic since we work on the differential state between diastole and systole so only the tangent behaviour of the stress-strain relationship was taken into account. We assumed a 2D plane strain problem in the finite deformation framework. Quasi static conditions were postulated because heart beat frequency was approximately 1 Hz.

The elastic properties of the surrounding tissue were set in the FE model to $E = 30$ kPa with a Poisson's ratio $\nu = 0.49$ [29]. The elastic properties of the "artificial" tissue were set to have no mechanical influence: $E = 10^{-6}$ kPa and $\nu = 0$. We checked that the presence of this artificial tissue in the FE model had no influence on the displacement fields. The Poisson's ratio of the CCA was set to $\nu = 0.49$. The elastic modulus of the artery was unknown and had to be recovered.

2.5 Identified variables

2.5.1 Elastic properties of the common carotid arteries

The aim of this study is first to study the elastic properties of the CCA. The other variables such as the mechanical properties of the surrounding material, the blood pressure, or the geometry of the FE model was supposed to be known. We further investigate the effects of these properties on the identified elastic properties of the artery. For one subject and one side, we performed a total of 5 different identifications of the elastic properties of the CCA, which comprise one identification for the diastole-systole average behaviour and 4 identifications at successive parts of the cardiac cycle in which the template and target images are chosen.

Table 2: Description of the 5 different couples of template/target images used for each hand side on each subject/patient.

Identification procedure	Template image	Target image
(a)	End-diastole	Mid-systole
(b)	Mid-systole	End-systole
(c)	Mid-diastole	End-systole
(d)	End-diastole	Mid-diastole
(e)	End-diastole	End-systole

The reader can refer to the Figure 4 for an illustration of the different identification times. The mid-systole time was defined as the time from the end-diastole to recover 50% of the systolic pressure. The same calculation was applied to recover the mid-diastole time. The procedures (a) to (d) in Table 2 describe the variation of the elastic properties through the cardiac cycle. The procedures (b) and (c) use the deformed FE model obtained at the end of the identification procedures (a) and (d), respectively. Note that only the geometry was imported and not the stress field. The imposed boundary conditions in pressure are described in Section 2.6. The procedure (e) uses the most deformed images that are, on the one hand the diastolic or initial image as the template, and on the other hand the systolic image as the target. In this case, the measured pulse pressure was applied.

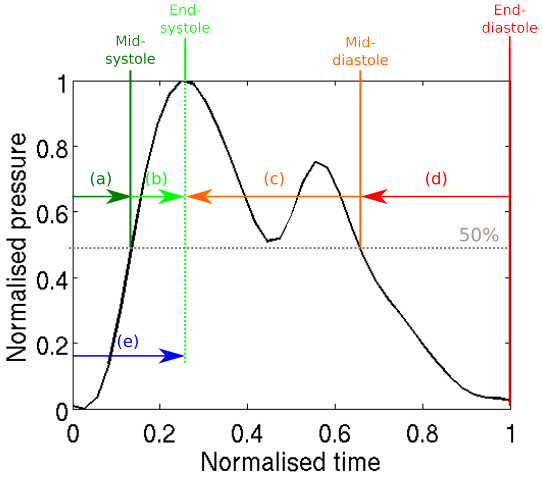

Figure 4: Illustration of the subsections of the cardiac cycle defined to identify 4+1 different elastic moduli throughout a cardiac cycle (identification procedures (a) to (d), the target and template images are chosen according to this scheme and the pressure applied as a boundary condition is the corresponding differential pressure). The identification procedures (b) and (c) use the deformed geometries obtained at the end of the identifications (a) and (d) respectively. For the procedures (c) and (d) the template image is taken later in time than the target image in order to keep a positive pressure inflation. The identification procedure (e) uses the measured pulse pressure as a boundary condition and the images at diastole and systole .

2.5.2 Correction of the in-plane translation

As described previously, the FE models were determined from the initial image. During the increase of pressure in the arterial tree, in-plane movements of the artery can potentially occur due the real complex 3D geometry. These movements are a translation of the artery in the cutting plane, that cannot be taken into account directly with our 2D FE model. Then, before each identification procedure, we estimated the in-plane translation of the artery by (i) first, defining a region of interest (ROI) on a "correction image" (template image registered with a displacement field of the FE model with $E_{artery} = 600$ kPa. This region of interest was a square that contains the artery. The square's limits were deduced from the binary mask used. (ii) Second, we performed a normalised cross-correlation between this ROI and the correction image, and this ROI and the target image. The difference between the

locations of the maximum of these normalised cross-correlations gives the estimated correction vector that is used throughout the identification procedure (see Figure 5). In summary, a complete identification procedure consists in the estimation of the in-plane translation of the artery, and then of the identification of the elastic properties of the CCA using the MB-FEMU method. The effect of this correction vector is discussed later in the article.

2.6 Determination of the blood pressure

The diastolic and systolic blood pressure were measured several times during the protocol. Different digital or manual sphygmomanometers were used. It was assumed that the pressure in the CCA is the same as the pressure measured in the brachial artery. For several subjects, the blood pressure was measured before, during and after the MR exam on the left arm. In addition to these measurements of the diastolic and systolic pressures, an applanation tonometry examination was performed. It consists in applying a probe on the neck of the subject/patient for obtaining the profile of pressure variations throughout a cardiac cycle. A second approach was designed here for obtaining this data. The approach consists in estimating an index, called the "P-index" for "Pressure index", based on the mean deformation of the artery throughout the cardiac cycle. The idea behind the P-index is that the instantaneous artery size, as measured by MRI, is representative of its internal pressure.

The P-index is determined for each subject and for each neck-side. Considering the 2D+t set of images, the first image (diastole state) is subtracted from every image frame for which the P-index has to be computed (see Figure 6). Then the P-index is defined as:

$$\begin{array}{rcl} \text{P-index}_{raw}\left(t\right) & = & \frac{1}{N_{pix}}\sum_{i=1}^{N_{pix}} I^i\left(t\right) - I^i\left(t_0\right) \\ \text{P-index}\left(t\right) & = & \frac{\text{P-index}_{raw}(t) - \min(\text{P-index}_{raw}(t))}{\max(\text{P-index}_{raw}(t)) - \min(\text{P-index}_{raw}(t))} \end{array} \quad (2)$$

where N_{pix} is the number of pixels of the binary mask (Figure 3); i is the i$^{\text{th}}$ pixel in this set of pixels; t_0 is the initial time (diastole).

Once the P-index is calculated, it is used to determine which image frame is respectively at the mid-systole time, end-systole time, mid-diastole time and end-

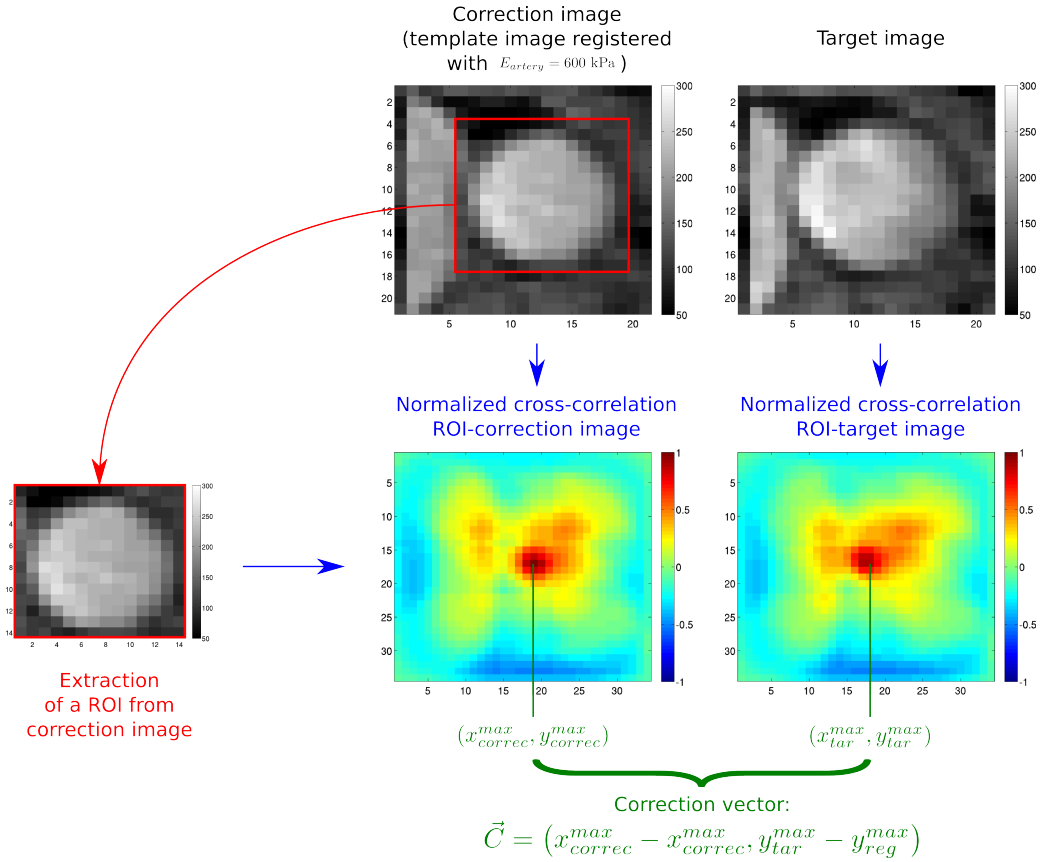

Figure 5: Principle of the correction of the translation between the template and the target image. The template image is first registered using an elastic modulus of the artery of 600 kPa. The ROI is chosen as the circumscribed square of the binary mask. A normalised cross-correlation between the ROI and the registered image gives a map where the maximum can be located. This corresponds to the location of the ROI in the registered image. The same operation is computed between the ROI and the target image to find the best location of the ROI in the target image. The difference between these two sets of coordinates gives the correction vector.

diastole time (see Figure 4). The end-diastole and end-systole images can be determined directly: the end-diastole image is the first image and the end-systole image is the image where the P-index reaches its maximum. The mid-states (mid-diastole and mid-systole) images were chosen when the P-index reaches 50 % of its maximal value.

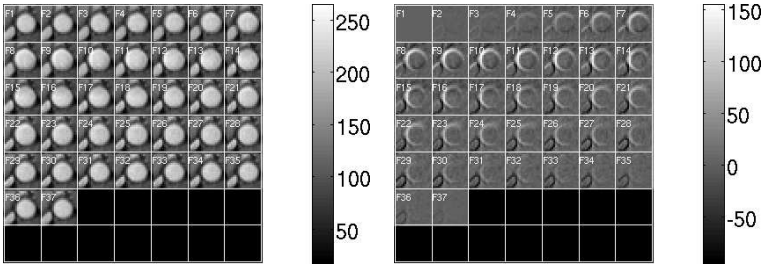

(a) Set of images throughout the cardiac cycle. This example is made up with 37 frames equally distributed throughout the cardiac cycle.

(b) The first image (diastole) is subtracted to every image frame.

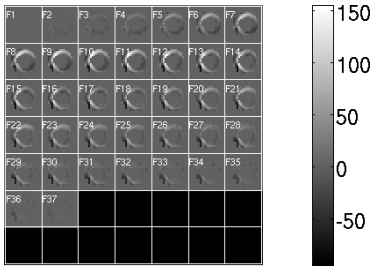

(c) The binary mask (Figure 3) is applied.

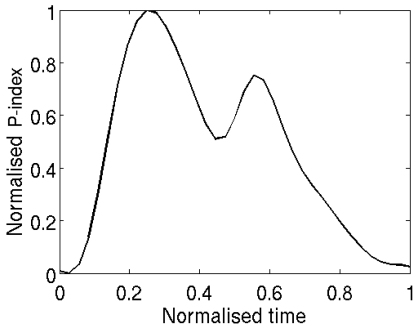

(d) Example of P-index profile throughout a cardiac cycle.

Figure 6: Principle of calculation of the P-index.

3 Results

3.1 Geometries of the subjects arteries

All the geometries were segmented independently. The diameter of the arteries was estimated from the cross-sectional area [4] of the 2D in-plane shape of the artery

277 ($D = 2\sqrt{(A/\pi)}$, see Figure 3). The mean diameter of the healthy arteries is
278 6.45 ± 0.70 mm while the 5 diseased arteries have a mean diameter of 6.66 ± 1.54 mm.

Table 3: Equivalent diameters of the arteries of the subjects taking part to the experiment.

Subject/ Patient	Diameters (mm) Left	Right
YH1	6.81	6.46
YH2	5.70	6.22
YH3	6.32	6.71
YH4	6.33	6.33
MAH1	6.05	6.60
MAH2	7.17	6.65
MAH3	7.40	6.25
MAH4	6.62	6.78
MAH5	5.45	5.39
OD1	5.57	5.06
OD2	6.00	6.64
OD3	8.48	9.04
OD4	5.68	7.01

279 The FE geometries were derived from the initial (diastole) image of each subject
280 (see A). The variability of neck morphologies is evident. Oblong shapes (YH1, YH2,
281 YH3, YH4, MAH1, MAH3, MAH5, OD1, OD4) and round shapes (OD2) can be
282 observed as well as more angular shapes (MAH2, MAH4, OD3). Jugular veins (the
283 internal jugular here) on a unique subject also present some variability. Two subjects
284 exhibit a split vein close to the artery on one side only (MAH4 and MAH5). The
285 vein is crushed for subjects YH4, MAH2 and MAH3 (one side), and for patient OD4.
286 The locations of the artery with regards to the spine also varies significantly (see
287 Table 4). On the average, this distance is 7 mm but it varies from 2 mm to 12 mm
288 between different individuals.

Table 4: Approximate distance between the spine and the inner contour of the CCA.

Subject/ Patient	Distance (mm) Vertebral column - artery	
	Left	Right
YH1	11	12
YH2	7	9
YH3	7	9
YH4	4	6
MAH1	2	6
MAH2	9	4
MAH3	7	5
MAH4	4	5
MAH5	10	10
OD1	7	6
OD2	4	7
OD3	5	9
OD4	12	12

3.2 Blood pressure

The results of the determination of the blood pressure in the CCA are shown in B. The P-index shows a profile that consists in a first rapid increase and then a decrease until reaching almost zero at the end-diastole state.

Differences between the P-index profiles and the pressure profiles obtained by applanation tonometry are significant. Figure 7 shows the difference in the initial slope defined as $(1 - \mathit{Slope}\ \text{P-index}/\mathit{Slope}\ \text{Tonometer}) \times 100$. On the average, there is a ratio between both initial slopes of -28.24 %. This ratio is of -67.41 ± 0.07 % for the YH group, -35.91 ± 14.08 % for the MAH group and -34.49 ± 33.37 % and 50.50 ± 72.99 % for the healthy and the diseased arteries of the OD group, respectively. These differences between initial slopes induce a time offset between the systole of the P-index and the systole from the pressure profile.

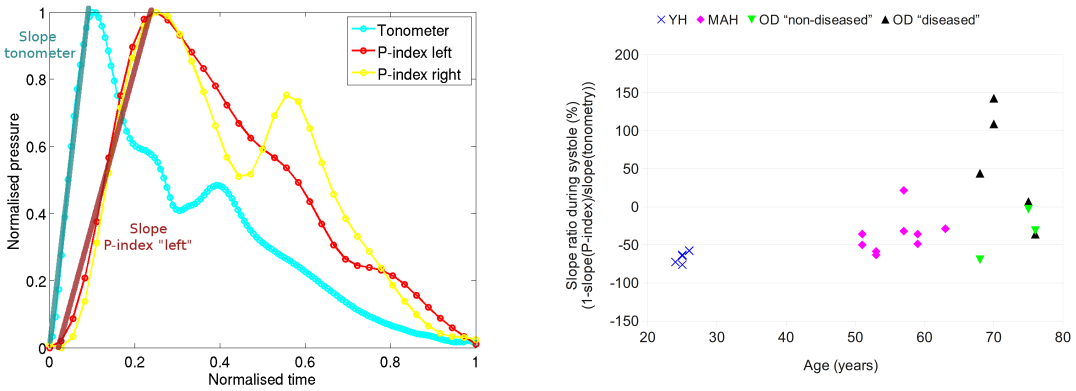

(a) Initial slopes of the pressure profile and of the P-index profile.

(b) Slope ratios for the young subjects (YH), the mid-age subjects (MAH) and the old patients (OD).

Figure 7: Comparison between the initial slopes of the P-index and of the tonometer pressure.

3.3 Identified elastic moduli

The values of the identified elastic moduli are reported in Table 5. An indicator of the quality of image registration is also reported, defined as:

$$DI = 100 \times \frac{J_2\left(E_{artery}^{identified}\right)}{J_2^{\infty}} \tag{3}$$

where J_2^{∞} corresponds to the distance between the target image and the template image (only across the binary mask). J_2^{∞} is the value of the objective function when neither deformation nor correction of displacement is allowed (see Figure 8). The DI index characterises the reduction of the cost function with the identification procedure.

Table 5: Identification results

Subject	Identification Procedure	Elastic modulus (kPa) Left	Elastic modulus (kPa) Right	DI (%) Left	DI (%) Right
YH1	(a)	221	192	25.79	13.27
	(b)	349	303	50.48	56.06
	(c)	455	193	38.86	23.94
	(d)	185	456	13.19	20.79
	(e)	289	325	8.08	11.61
YH2	(a)	147	395	38.45	63.74
	(b)	662	213	88.69	56.39
	(c)	236	234	51.84	63.93
	(d)	208	347	43.36	55.38
	(e)	228	288	25.95	38.89
YH3	(a)	177	204	30.72	33.19
	(b)	793	1890	75.33	86.36
	(c)	250	308	34.03	31.24
	(d)	322	374	19.21	27.26
	(e)	318	363	10.15	14.85
YH4	(a)	132	119	23.82	40.93
	(b)	228	187	53.66	53.00
	(c)	230	128	50.43	38.20
	(d)	129	134	15.75	27.33
	(e)	224	490	36.21	21.83
MAH1	(a)	211	934	58.18	33.25
	(b)	499	848	86.33	28.99
	(c)	246	317	76.99	73.64
	(d)	292	167	55.06	17.83
	(e)	265	921	53.47	35.47
MAH2	(a)	374	338	51.17	47.84
	(b)	640	801	71.91	81.89

Continued on next page

Table 5 – *Continued from previous page*

Subject	Identification Procedure	Elastic modulus (kPa) Left	Elastic modulus (kPa) Right	DI (%) Left	DI (%) Right
	(c)	423	580	69.01	71.07
	(d)	401	364	42.40	47.71
	(e)	446	464	40.61	42.84
MAH3	(a)	368	264	64.76	80.53
	(b)	503	574	83.25	88.03
	(c)	367	258	76.15	82.68
	(d)	448	604	72.20	86.64
	(e)	483	520	54.71	73.13
MAH4	(a)	200	386	49.69	66.78
	(b)	10843	1057	99.06	84.96
	(c)	454	545	64.76	62.84
	(d)	598	625	67.18	61.08
	(e)	503	563	35.85	47.30
MAH5	(a)	445	1281	47.55	13.95
	(b)	357	290	90.54	62.87
	(c)	642	1013	81.72	54.61
	(d)	285	245	56.89	59.61
	(e)	420	502	55.03	15.64
OD1	(a)	8781	5418	98.12	94.40
	(b)	600	7727	124.07	98.01
	(c)	50000	600	100.36	100.00
	(d)	812	655	68.39	74.65
	(e)	2239	6423	96.14	94.66
OD2	(a)	229	449	68.16	53.92
	(b)	213	724	55.81	89.48
	(c)	325	437	55.13	83.50
	(d)	406	491	67.54	69.42

Continued on next page

Table 5 – *Continued from previous page*

Subject	Identification Procedure	Elastic modulus (kPa) Left	Elastic modulus (kPa) Right	DI (%) Left	DI (%) Right
	(e)	392	487	41.57	58.14
OD3	(a)	953	1165	53.01	70.07
	(b)	1117	2532	89.51	83.41
	(c)	1311	2065	79.96	81.01
	(d)	727	2098	64.92	71.35
	(e)	906	1308	61.56	62.04
OD4	(a)	235	528	64.02	78.11
	(b)	1499	424	97.51	68.14
	(c)	591	540	88.56	80.16
	(d)	376	577	70.94	69.53
	(e)	456	549	75.05	53.07

309

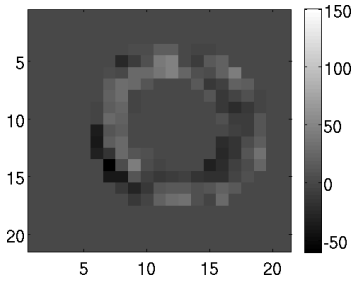

(a) Difference between the registered and the target images

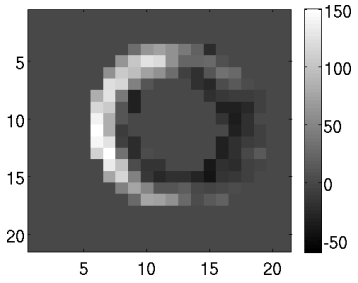

(b) Difference between the template and target images

Figure 8: Difference between the target image and (a) the registered image after the identification or (b) the template image.

3.3.1 Elastic modulus

Using the MB-FEMU method, the elastic moduli of the CCA (left and right) of each subject is identified. First, we calculated the global modulus throughout the whole cardiac cycle. The global modulus is estimated with the diastole image as template image and the systole image as target image. The pressure which is applied as a boundary condition in the model is the difference between diastolic and systolic pressures measured on each subject.

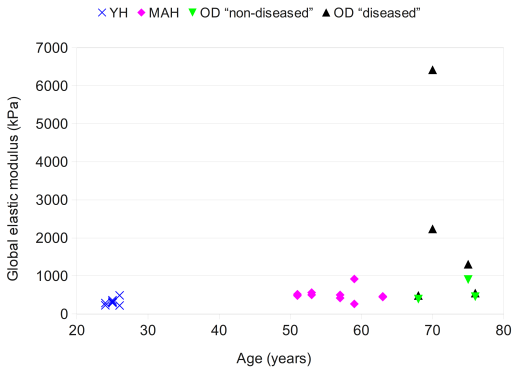

Figure 9: Global elastic modulus identified throughout a whole cardiac cycle.

Effect of age and disease The results show an increase in the elastic modulus of the CCA with age and disease (see Figure 9). The YH group exhibits a mean elastic modulus of 315 ± 29 kPa. It is 38 % inferior to the mean modulus of the MAH group (509 ± 65 kPa). The means of the OD group has not been calculated due to a lack of data.

Effect of the surrounding tissue It has been shown previously that, through a stiffness compensation effect, the identified elastic modulus of the CCA E_{artery} using the MB-FEMU is influenced by the estimation of the elastic properties of the surrounding tissue $E_{surrounding}$ [10]. Figure 10a shows how the estimation of these elastic properties can affect the identified elastic properties of the artery, E_{artery}. If E_{artery} when $E_{surrounding} = 30$ kPa is taken as a reference, E_{artery} is overestimated by 19 %

when $E_{surrounding} = 1$ kPa and underestimated by -18 % when $E_{surrounding} = 60$ kPa on the average (excluding OD1 and OD3). The relationship between $E_{surrounding}$ and E_{artery} is linear in most of cases (25/26 arteries show a Pearson's correlation coefficient (PCC) $r < -0.9$). It is particularly the case for the YH group who have a mean PCC $r < -0.99$. The non-diseased arteries of the OD group present the worst coefficient $r = -0.39$ but there are only 3 specimens and the values are scattered (from $r = -1$ to $r = 0.82$).

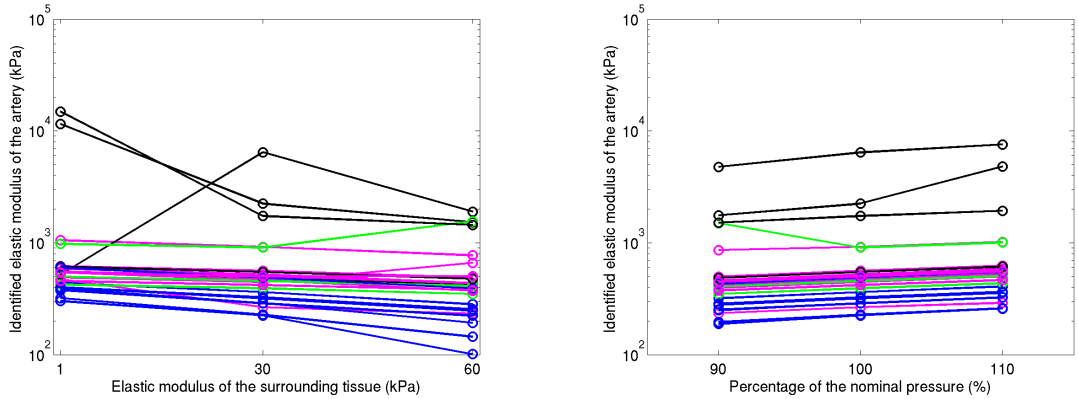

(a) Influence of the elastic modulus of the surrounding tissue. The elastic modulus of the surrounding tissue has been changed in the FE model from 1 kPa to 60 kPa.

(b) Influence the estimated blood pressure. The applied blood pressure has been under or over estimated by 10%.

Figure 10: Influence on the global identified elastic modulus of the estimation of (a) the elastic modulus of the surrounding tissue and (b) the estimated blood pressure (YH: blue; MAH: magenta; OD non-diseased/diseased: green/black).

Effect of the pressure The pressure has a similar effect on the identified elastic modulus since it participates to the boundary conditions of the FE model. E_{artery} is underestimated by -10 % with a pressure underestimation of -10 %. When the pressure is overestimated by $+10$ %, E_{artery} is overestimated by $+12$ % (excluding OD1).The PCC with regards to the evolution of the pressure applied is $r = 0.99$ excluding the left hand side of OD3 (negative coefficient).

3.3.2 Evolution of the elastic modulus during a cardiac cycle

We have then identified elastic moduli at different times of the cardiac cycle:

a Between the diastole and the mid-systole

b Between the mid-systole and the systole

c Between the systole and the mid-diastole

d Between the mid-diastole and the diastole

Each modulus is estimated with the appropriate template and target images determined from the considered fraction of the cardiac cycle. The pressures which are applied as boundary conditions in the model are calculated using the P-index profiles. Results are shown in Figure 11 for the YH, MAH and OD group. The identification in the OD1 case has been excluded because it has failed, which numerically means that the Levenberg-Marquardt algorithm stops due to a null gradient and $DI > 100$ %.

The YH group has an average elastic modulus of 325 kPa over the whole cardiac cycle whereas the MAH group has an average elastic modulus of 752 kPa. The value of the elastic modulus for the YH group starts from 198 kPa during the first fraction of the cardiac cycle (see Figure 4), then it increases to 578 kPa in the second fraction of the cardiac cycle, and is finally stable in the two last fractions until the return to the diastole state (254 kPa and 269 kPa). The evolution of the elastic modulus of the artery through the cardiac cycle is similar for the MAH group, with a higher elastic modulus in the (b) fraction of the cardiac cycle than in the (a) fraction (619 kPa on the average versus 511 kPa, excluding MAH4), and a stable modulus during the diastolic phase ((c): 488 kPa on the average, (d): 381 kPa) (see Figure 11e). The number of data for the OD group is very limited so that the means are not meaningful.

4 Discussion

4.1 Effect of the age and of disease on the stiffness

The results show that there is an increase of +38% of the global elastic modulus of the artery between the YH group and the MAH group. A Student's t-test on the identified modulus of Table 5 (identification procedure (e)) reveals a significant difference between the means of these two groups with a p-value[1] $p = 0.9968$ [2]. These findings are in agreement with the literature. The large study of [30] shows that there was a significant increase of the stiffness of the carotid arteries for males and females from 40 years old to 64 years old. This increase has also been pointed out in the review of [26]. The low number of data points for old and diseased patients renders difficult the interpretation of the mean values, and other experiments should be conducted. We can note that the diseased artery is always stiffer than the non-diseased artery for patients OD2, OD3 and OD4 who have a unilateral lesion (392 kPa vs 487 kPa, 906 kPa vs 1732 kPa, 456 kPa vs 549 kPa, respectively).

4.2 Comparision between the P-index profile and pressure profiles obtained by the applanation tonometry technique

It is interesting to see the differences between the blood pressure measured by applanation tonometry and the P-index profiles. For all cases excepted the old diseased patients, the pressure increase as seen through the P-index is slower than that seen by tonometry. These differences could be explained by the possible inertia of the artery to be deformed or by the MRI artefacts. Figure 7 reveals that the difference of slope between the P-index and the tonometry during the systole evolves with age and disease in the same way as the stiffness of the artery: YH$<$MAH ($p = 0.9989$),

[1] the p-value is the probability of having an observation at least as extreme as the observation if the hypothesis H0 is true. Low p-values (lower than a chosen significance level) may induce a rejection of H0.

[2] data fit a standard distribution, the variances are assumed to be unequal (Behrens-Fisher problem [18]), unilateral test with the null hypothesis H_0: "mean from data set 1 is lower than mean from data set 2"

MAH<non-diseased OD ($p = 0.5248$), non-diseased OD<diseased OD ($p = 0.9698$)[3].

4.3 Evolution of elastic properties throughout the cardiac cycle

Arteries are known to be nonlinear [11, 13]. Since we have considered a linear mechanical behaviour, we have identified different elastic properties at different fractions of the cardiac cycle. Note that there is a clear increase of the elastic modulus just before the end-systole (identification at the (b) part of the cardiac cycle) for both the YH group ($p = 0.95$) and the MAH group ($p = 0.74$)[4]. There is also a significant decrease of the elastic modulus during the return to diastole (identification at the (c) part of the cardiac cycle) for both groups ($p = 0.93$ and $p = 0.82$, respectively[5]).The decrease of the elastic modulus between the cardiac cycle parts (c) and (d) is not clear ($p = 0.40$ and $p = 0.83$ for the YH group and the MAH group, respectively). We have also seen that the moduli from the identification procedures (a), (c) and (d) are relatively close for both groups (198 $\rightarrow$ 269 kPa and 381 $\rightarrow$ 488 kPa, respectively). In both groups the elastic modulus is minimum during the first part of the cardiac cycle, then increases during systole, and finally decreases during the return to diastole and goes back to its initial value for the identification procedure (d). The lack of data on the OD group has prevented to perform the t-tests. Other authors were able to observe the differences between the elastic modulus of the artery at diastole and systole: [8] have studied the propagation of shear waves in arteries using ultrasounds. They found on a unique subject that the elastic modulus steps up from 258 kPa during diastole to 402 kPa during systole. It is an increase of +56 % which is less than what we found on the YH group (+191 %) and higher than what we found on the MAH group (+21 %). Interestingly, the tested subject was 30 years old while the mean age of the YH group was 25 years old and the mean age of the

[3] unpaired Student's t-test, data fit a standard distribution, the variances are assumed to be unequal, unilateral test with the null hypothesis H_0: "mean from data set 1 is lower than mean from data set 2"

[4] paired Student's t-test, the difference between the paired data fit a standard distribution, unilateral test with the null hypothesis H_0: "mean from data set 1 is lower than mean from data set 2")

[5] null hypothesis H_0: "mean from data set 1 is higher than mean from data set 2"

MAH group was 57 years old.

4.4 On the importance of an accurate measurement of the blood pressure

Results from Section 3.3.1 and previous tests on the MB-FEMU method [10] have pointed out the major role of the blood pressure for the estimation of the artery's stiffness *in vivo*. We have found that the identified elastic modulus of the artery is directly influenced by how the blood pressure is measured. In the literature, many authors used a direct formula that links the elastic modulus to the variation of diameter of the artery [30, 21]. The effect of the measurement of pressure is then also crucial. In a previous article [10] we noticed the substantial variation of the pulse pressure of a subject just before the MRI and 15 minutes after the exam (pulse pressure $P_{MRI} = 85$ mmHg vs $P_{MRI+15\text{ min}} = 62$ mmHg) while the normal value is $P = 40$ mmHg. In the present study, the blood pressure of three healthy subjects was measured every 2 minutes using a programmable digital sphygmomanometer throughout the whole MR exam. An inflation armband was fixed on the arm of the subject before the exam. The results are shown in Figure 12. They reveal significant changes of the blood pressure during the MR exam. These changes may be explained in part by the stress provoked by the exam. We can see on the curves that MAH2 has apparently increased his systolic and diastolic pressures after 18 minutes in the MRI. This increase is correlated to the start of the PC sequence which is very noisy due to the flip of the magnetic field. On the contrary, the diastolic and systolic pressures of MAH3 and MAH4 are relatively stable, with a tendency to decrease. If we look at the pulse pressure, and if we consider the mean pulse pressure of each subject as the reference, the variation is very important during the exam (-17 % / $+14$ % for MAH2, -21 % / $+18$ % for MAH3 excluding the first data, -15 % / $+12$ % for MAH4). This variation of blood pressure has also consequences on images because it introduces blur on the contour of the artery: indeed each frame image is the reconstruction of a k-space which has been filled during several cardiac cycles [5]. If the blood pressure was different between the cardiac cycles, the displacement of the artery would also be different. This could explain the special shapes of the P-index

for certain subjects and patients (YH4, MAH3, MAH4, MAH5, OD2).

Moreover in this study we considered that the pulse pressure in the CCA was identical to the pulse pressure in the brachial artery. In reality, it has been reported that the pulse pressure in the brachial is typically larger to that in the CCA by about $10 - 14$ mmHg [32, 31]. In our case it means that the identified moduli are slightly overestimated. The applanation tonometry exam could estimate the pulse pressure in the carotid after a proper calibration [34, 20], but it has not been used here because the procedures are time consuming and not compatible with our clinical conditions.

4.5 Assumptions made within the Finite Element Model

In this study, as well as in our previous work [10], we have underlined the influence of the mechanical properties of the surrounding tissue. The elastic properties of the surrounding tissue can be potentially identified simultaneously with the elastic properties of the artery as in [22]. But this induces several difficulties: (i) The total identification time is multiplied by three. (ii) The solution is potentially not unique, whereas it is the case when only one modulus is identified. (iii) The obtained solutions can be meaningless with regard to the physics. Here the choice of a homogeneous model of the surrounding tissue is not realistic. The surrounding medium is much more complex and heterogeneous (muscle, tendons, fascias, etc.) but since we focused only on the mechanical properties of the artery we have chosen not to refine the FE model. In addition, the correction of images that occurs at the beginning of each identification procedure has been designed to incorporate rigid displacements that are due to the real 3D geometry of the neck. Our implementation was fast and simple. It is then possible to recover the coordinates of the correction vector simultaneously with the elastic properties of the artery with a limited impact on the total identification time since no additional FE computation is necessary. The geometry of the FE models is important because it imposes strong constraints on the registration framework. We have seen that the diameters of the arteries and more generally the morphologies of the subjects and patients differ significantly from one subject to another and even among the subjects and patients themselves. But

no correlation appears between the diameter of the artery and the identified elastic modulus, or between the distance between the artery and the spine and the elastic modulus. This means that the geometry of the FE model is crucial for an accurate identification, but its influence on the mean identified elastic modulus is limited. Other approaches such as the "hyperelastic warping" [35] exist which, by releasing some of the assumptions on the geometry, could improve the results.

4.6 Limitation

Two words of caution are needed for clinical use of the proposed identification method. First, if the patient is taking medications that affect the mechanical properties of the arteries such as beta-blockers, the identified mechanical properties of the arteries will include the effect of the medication. If the patient is taking medications that affect the blood pressure without changing the mechanical properties of the arteries, the method will correctly identify the mechanical properties of the arteries because the actual blood pressure is estimated and used as a boundary condition. Second, if the patient suffers severe cardiac rhythm disorders, the MRI images can be blurred because a single image is reconstructed from images taken during several cardiac cycles [5, 1]. In this case, a finer analysis of the MRI reconstruction method coupled with accurate *in situ* blood pressure measurements could be appropriate but such research topic is out of the scope of this work.

5 Conclusion

In this study we successfully applied the MB-FEMU method [10] for identifying the *in vivo* elastic moduli of the common carotid arteries of 13 healthy subjects and sclerosed patients from 24 to 76 years old based on data provided by cine MRI. These data have been obtained in clinical conditions from existing Phase Contrast MR sequence. This approach requires to record at the same time the blood pressure. An increase of the artery's stiffness with age and atherosclerosis has been observed. More experiments are however needed to determine if the diseased arteries can be distinguished from non-diseased arteries based on the analysis of stiffness. The vari-

ation of the elastic modulus of the artery during a single cardiac cycle has also been observed and a stiffening of the artery during systole has been underlined. This opens the door to the identification of the nonlinear mechanical properties of the artery *in vivo*. Additional steps are nevertheless required, such as the necessity of a very accurate measurement of the blood pressure, and the use of an appropriate FE model with a refined surrounding media. The MB-FEMU method is promising for the identification of heterogeneous and complex *in vivo* mechanical properties of any artery, and the application of this method on atherosclerosed sites could improve our knowledge about the biomechanical properties of plaques.

Acknowledgements

This work is part of the Imandef Project (*in vivo* mechanical identification of tissues using medical imaging, grant ANR-08-JCJC-0071) funded by the ANR (French National Research Agency). We would like to thank the volunteers for their time and implication.

We would like to thank the Journal of the Mechanical Behaviour of Biomedical Materials (please visit http://www.journals.elsevier.com/journal-of-the-mechanical-behavior-of-biomedical-materials/).

References

[1] M. A. Bernstein, K. F. King, and X. J. Zhou. *Handbook of MRI pulse sequences*. Elsevier Inc., 2004.

[2] P. Boutouyrie, D. P. Germain, J-N. Fiessinger, B. Laloux, J. Perdu, and S. Laurent. Increased Carotid Wall Stress in Vascular Ehlers-Danlos Syndrome. *Circulation*, 109(12):1530–1535, 2004.

[3] P. Boutouyrie, D. P. Germain, A-I. Tropeano, B. Laloux, F. Carenzi, M. Zidi, X. Jeunemaitre, and S. Laurent. Compressibility of the Carotid Artery in Patients With Pseudoxanthoma Elasticum. *Hypertension*, 38(5):1181–1184, 2001.

[4] P. J. Brands, A. P. G. Hoeks, J. Willigers, C. Willekes, and R. S. Reneman. An integrated system for the non-invasive assessment of vessel wall and hemodynamic properties of large arteries by means of ultrasound. *Eur J Ultrasound*, 9:257–266, 1999.

[5] M. A. Brown and R. C. Semelka. *MRI: basic principles and applications*. John Wiley & Sons, Inc., Hoboken, New Jersey, 3rd edition, 2003.

[6] C. Bussy, P. Boutouyrie, P. Lacolley, P. Challande, and S. Laurent. Intrinsic stiffness of the carotid arterial wall material in essential hypertensives. *Hypertension*, 35(5):1049–1054, 2000.

[7] L. E. Chambless, A. R. Folsom, L. X. Clegg, A. R. Sharrett, E. Shahar, F J. Nieto, W. D. Rosamond, and G. Evans. Carotid Wall Thickness is Predictive of Incident Clinical Stroke. *Am J Epidemiol*, 151(5):478–487, 2000.

[8] M. Couade, M. Pernot, C. Prada, E. Messas, J. Emmerich, P. Bruneval, A. Criton, M. Fink, and M. Tanter. Quantitative assessment of arterial wall biomechanical properties using shear wave imaging. *Ultrasound Med Biol*, 36(10):1662–1676, 2010.

[9] A. Franquet, S. Avril, R. Le Riche, and P. Badel. Identification of heterogeneous elastic properties in stenosed arteries: a numerical plane strain study. *Comput Methods Biomech Biomed Engin*, 15(1):49–58, 2012.

[10] A. Franquet, S. Avril, R. Le Riche, F. C. Schneider, P. Badel, C. Boissier, and Z-Y. Li. A new method for the in vivo identification of mechanical properties in arteries from cine MRI images: theoretical framework and validation. *IEEE Trans Med Imaging*, 2012.

[11] Y. C. Fung. *Biomechanics : Mechanical properties of living tissues*. Springer-Verlag, New-York, 2nd edition, 1993.

[12] F. Guyon and R. Le Riche. Least Squares Parameter Estimation and the Levenberg-Marquardt Algorithm : Deterministic Analysis, Sensitivities and

Numerical Experiments. Technical report, Institut National des Sciences Appliquées, 2000.

[13] G. A. Holzapfel. Biomechanics of Soft Tissues with Application to Arterial Walls. In J. A. C. Martins and E. A. C. Borges Pires, editors, *Mathematical and Computational Modeling of Biological Systems*, pages 1–37. Centro Internacional de Matemática CIM, 2002.

[14] J. L. Izzo and B. E. Shykoff. Arterial Stiffness: Clinical Relevance, Measurement, and Treatment. *Rev Cardiovasc Med*, 2(1):29–40, 2001.

[15] A. V. Kamenskiy, Y. A. Dzenis, J. N. MacTaggart, T. G. Lynch, S. A. Jaffar Kazmi, and I. I. Pipinos. Nonlinear mechanical behavior of the human common, external, and internal carotid arteries in vivo. *J Surg Res*, 176(1):329–336, 2012.

[16] T. Khamdaeng, J. Luo, J. Vappou, P. Terdtoon, and E. E. Konofagou. Arterial stiffness identification of the human carotid artery using the stress-strain relationship in vivo. *Ultrasonics*, 52(3):402–411, 2012.

[17] K. Kim, W. F. Weitzel, J. M. Rubin, H. Xie, X. Chen, and M. O'Donnell. Vascular intramural strain imaging using arterial pressure equalization. *Ultrasound Med Biol*, 30(6):761–771, 2004.

[18] S-H. Kim and A. S. Cohen. On the Behrens-Fisher Problem: A Review. *J Educ Behav Stat*, 23(4):356–377, 1998.

[19] B. A. Kingwell, T. K. Wadell, T. L. Medley, J. D. Cameron, and A. M. Dart. Large artery stiffness predicts ischemic threshold in patients with coronary artery disease. *J Am Coll Cardiol*, 40(4):773–779, 2002.

[20] J. Kips, F. Vanmolkot, D. Mahieu, S. Vermeersch, I. Fabry, J. de Hoon, L. Van Bortel, and P. Segers. The use of diameter distension waveforms as an alternative for tonometric pressure to assess carotid blood pressure. *Physiol Meas*, 31(4):543–553, 2010.

[21] S. Laurent, X. Girerd, J. J. Mourad, P. Lacolley, L. Beck, P. Boutouyrie, J. P. Mignot, and M. Safar. Elastic modulus of the radial artery wall material is not increased in patients with essential hypertension. *Arterioscler Thromb*, 14(7):1223–1231, 1994.

[22] S. Le Floc'h. *Modulographie vasculaire : Application à l'identification in-vivo du module de Young local des plaques d'athérosclérose*. PhD thesis, Université Joseph Fourier (Grenoble I), 2009.

[23] H. Liu, G. Canton, C. Yuan, C. Yang, K. Billiar, Z. Teng, A. H. Hoffman, and D. Tang. Using In Vivo Cine and 3D Multi-Contrast MRI to Determine Human Atherosclerotic Carotid Artery Material Properties and Circumferential Shrinkage Rate and Their Impact on Stress/Strain Predictions. *J Biomech Eng*, 134(1):011008, 2012.

[24] Y. Liu, C. Dang, M. Garcia, H. Gregersen, and G. S. Kassab. Surrounding tissues affect the passive mechanics of the vessel wall: theory and experiment. *Am J Physiol Heart Circ Physiol*, 293(6):H3290–3300, 2007.

[25] I. Masson, P. Boutouyrie, S. Laurent, J. D. Humphrey, and M. Zidi. Characterization of arterial wall mechanical behavior and stresses from human clinical data. *J Biomech*, 41(12):2618–2627, 2008.

[26] M. F. O'Rourke, J. A. Staessen, C. Vlachopoulos, D. Duprez, and G. E. Plante. Clinical applications of arterial stiffness; definitions and reference values. *Am J Hypertens*, 15(5):426–444, 2002.

[27] D. W. Park, M. S. Richards, J. M. Rubin, J. Hamilton, G. H. Kruger, and W. F. Weitzel. Arterial elasticity imaging: comparison of finite-element analysis models with high-resolution ultrasound speckle tracking. *Cardiovasc Ultrasound*, 8:22, 2010.

[28] E. Peña, V. Alastrué, A. Laborda, M. A. Martínez, and M. Doblaré. A constitutive formulation of vascular tissue mechanics including viscoelasticity and softening behaviour. *J Biomech*, 43(5):984–989, 2010.

[29] D. Périé, C. E. Aubin, M. Lacroix, Y. Lafon, and H. Labelle. Biomechanical modelling of orthotic treatment of the scoliotic spine including a detailed representation of the brace-torso interface. *Med Biol Eng Comput*, 42(3):339–344, 2004.

[30] W. A. Riley, R. W. Barnes, G. W. Evans, and G. L. Burke. Ultrasonic Measurement of the Elastic Modulus of the Common Carotid Artery. *Stroke*, 23(7):952–956, 1992.

[31] M. E. Safar and J. Blacher. Carotid Versus Brachial Pulse Pressure in Elderly Persons. *J Am Coll Cardiol*, 51(25):2440–2441, 2008.

[32] M. E. Safar and A. Kakou. Carotid and brachial blood pressure – measurements in hypertensive subjects. *Revista Brasileira de hipertensao*, 15(3):122–124, 2008.

[33] H. Tomiyama, T. Arai, Y. Koji, M. Yambe, K. Motobe, G. Zaydun, Y. Yamamoto, S. Horu, and A. Yamashina. The age related increase in arterial stiffness is augmented in phases according to the severity of hypertension. *Hypertens Res*, 27(7):465–470, 2004.

[34] F. Verbeke, P. Segers, S. Heireman, R. Vanholder, P. Verdonck, and L. M. Van Bortel. Noninvasive assessment of local pulse pressure: importance of brachial-to-radial pressure amplification. *Hypertension*, 46(1):244–248, 2005.

[35] A. I. Veress, N. Phatak, and J. A. Weiss. Deformable Image Registration with Hyperelastic Warping. In J S Suri, D L Wilson, and S Laxminarayan, editors, *Handbook of Biomedical Image Analysis*, pages 487–534. Kluwer Academic/Plenum, New-York, 3rd edition, 2004.

[36] C. W. Washington and M. I. Miga. Modality independent elastography (MIE): a new approach to elasticity imaging. *IEEE Trans Med Imaging*, 23(9):1117–1128, 2004.

[37] A. Wykretowicz, P. Gerstenberger, P. Guzik, A. Milewska, T. Krauze, K. Adamska, A. Rutkowska, and H. Wysocki. Arterial stiffness in relation to subclinical atherosclerosis. *Eur J Clin Invest*, 39(1):11–16, 2009.

[38] X. Zhang and J. F. Greenleaf. The stiffening of arteries by the tissue-mimicking gelatin. *IEEE Trans Ultrason Ferroelectr Freq Control*, 53(8):1534–1539, 2006.

A Finite element models for subjects and patients

See Figures 13, 14 and 15.

B Evolution of the blood pressure by applanation tonometry and P-index

See Figures 16, 17 and 18.

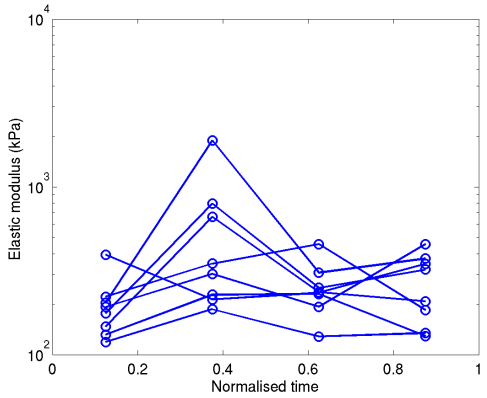

(a) Young healthy subjects

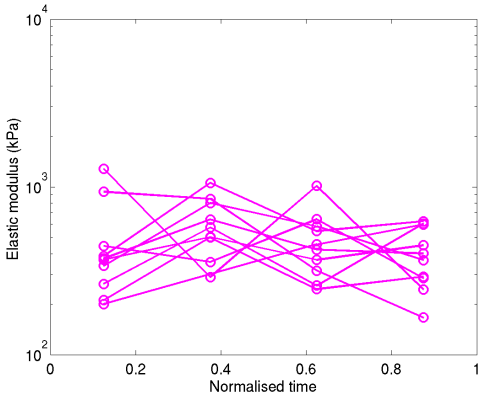

(b) Mid-age healthy subjects

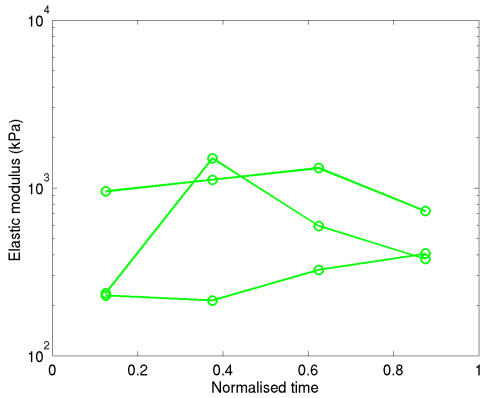

(c) Old diseased patients with non-diseased arteries

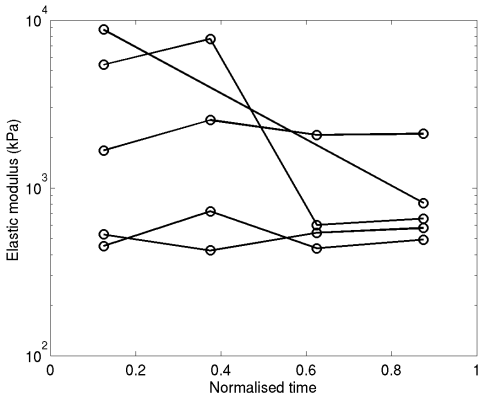

(d) Old diseased patients with diseased arteries

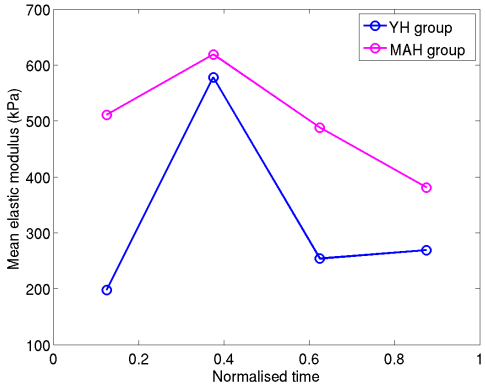

(e) Mean elastic moduli identified for the YH and the MAH groups at each time of the cardiac cycle.

Figure 11: Evolution of the elastic modulus during the cardiac cycle. The different points correspond to different fractions of the cardiac cycle.

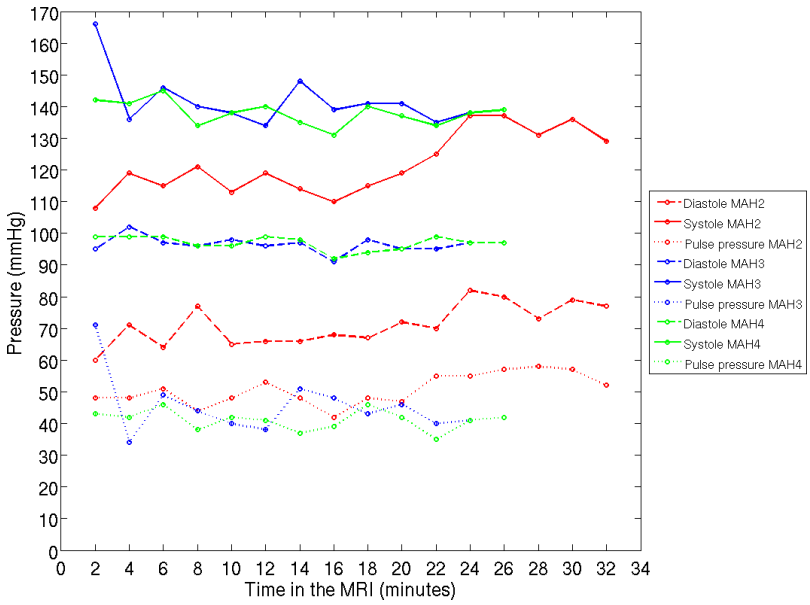

Figure 12: Evolution of the blood pressure during the MR exam for three healthy subjects. The blood pressure has been recorded every two minutes using a programmable digital sphygmomanometer.

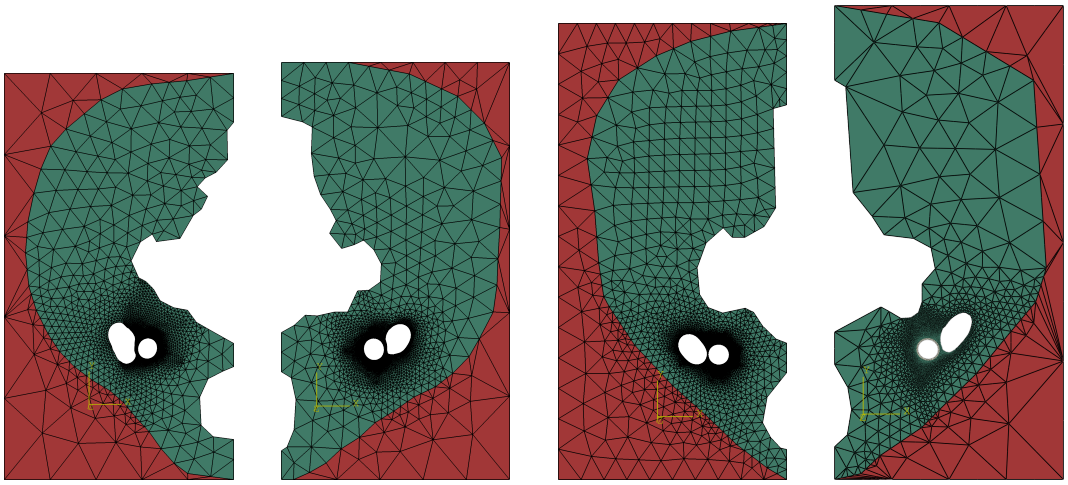

(a) Right YH1 (b) Left YH1 (c) Right YH2 (d) Left YH2

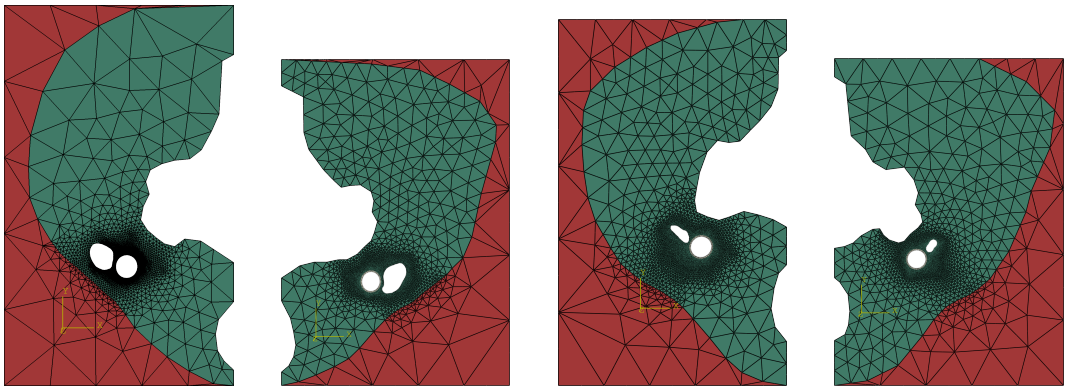

(e) Right YH3 (f) Left YH3 (g) Right YH4 (h) Left YH4

Figure 13: FE models of the "Young Healthy subjects" (YH) group. Note that the radiological convention has been used so left and right hand sides are reversed from the common usage.

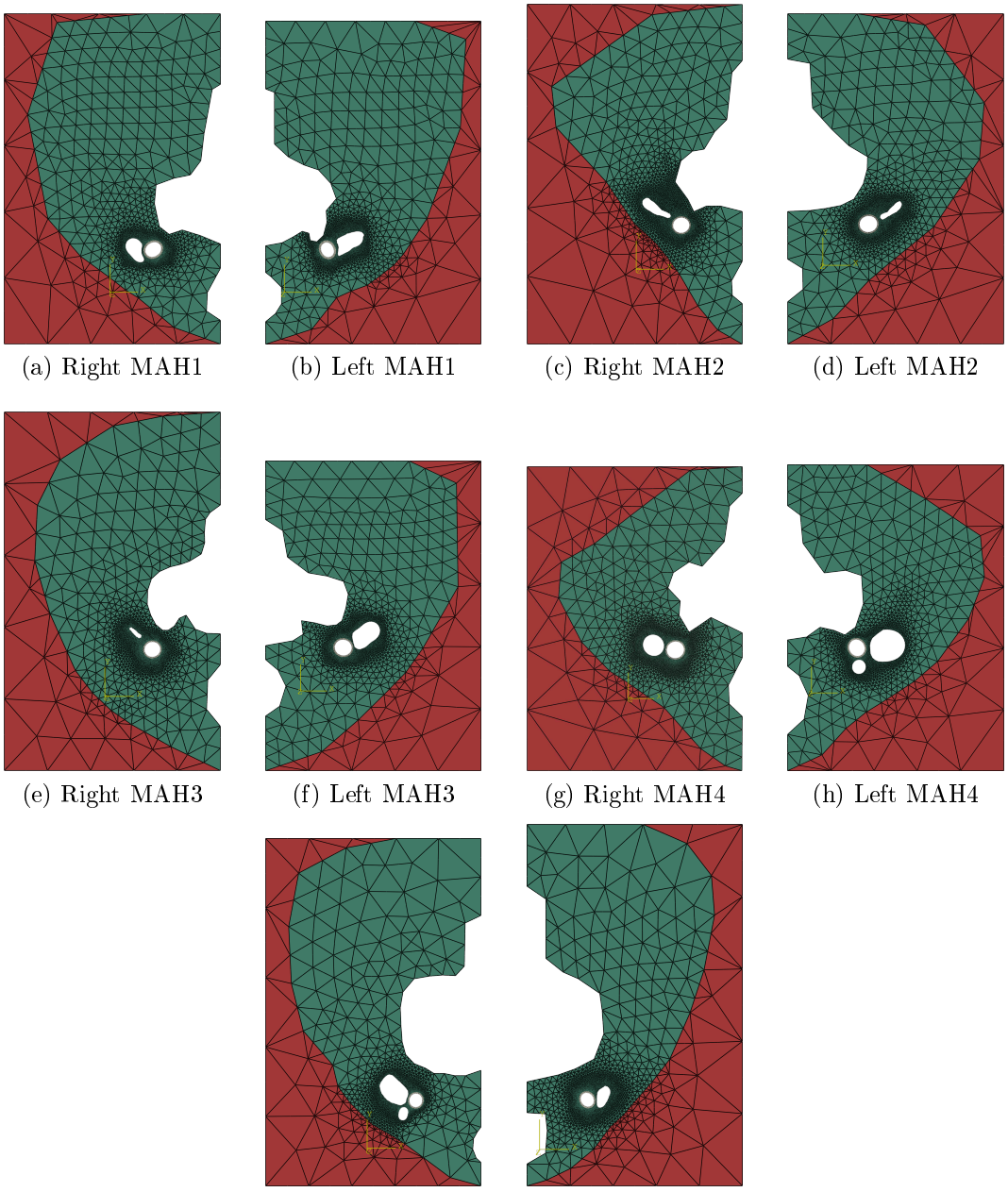

(a) Right MAH1 (b) Left MAH1 (c) Right MAH2 (d) Left MAH2

(e) Right MAH3 (f) Left MAH3 (g) Right MAH4 (h) Left MAH4

(i) Right MAH5 (j) Left MAH5

Figure 14: FE models of the "Mid-Age Healthy subjects" (MAH) group. Note that the radiological convention has been used so left and right hand sides are reversed from the common usage.

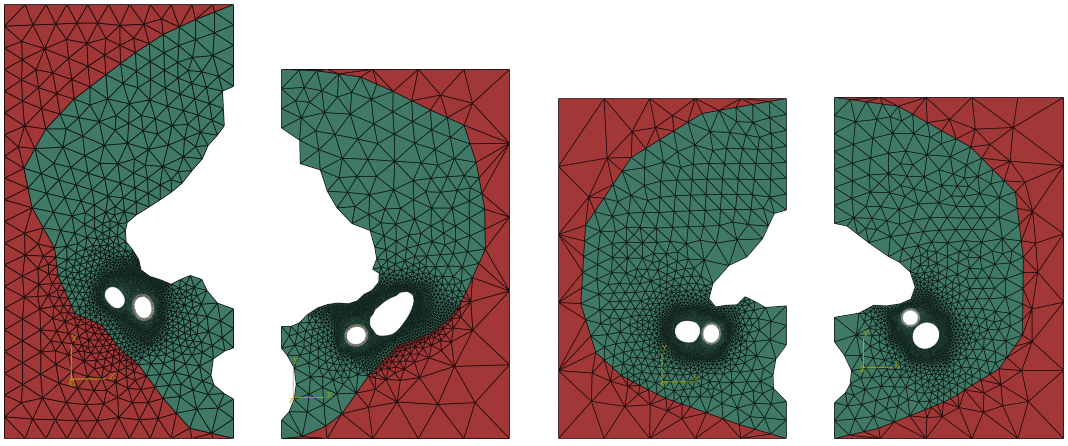

(a) Right OD1 (b) Left OD1 (c) Right OD2 (d) Left OD2

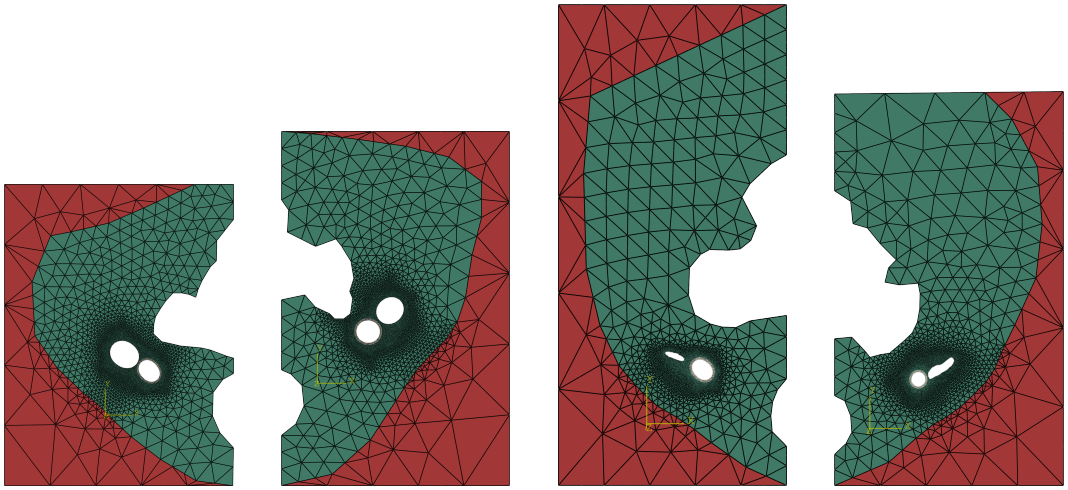

(e) Right OD3 (f) Left OD3 (g) Right OD4 (h) Left OD4

Figure 15: FE models of the "Old Diseased patients" (OD) group. Note that the radiological convention has been used so left and right hand sides are reversed from the common usage.

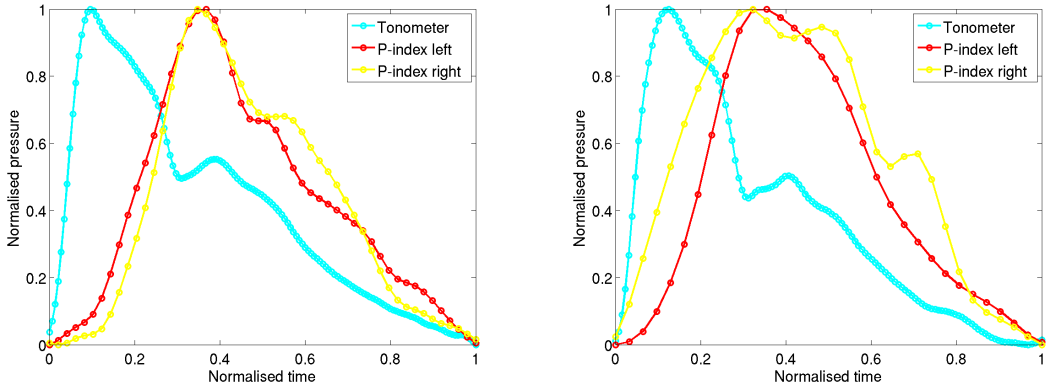

(a) YH1

(b) YH2

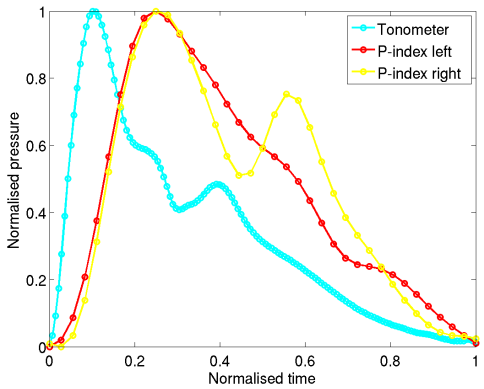

(c) YH3

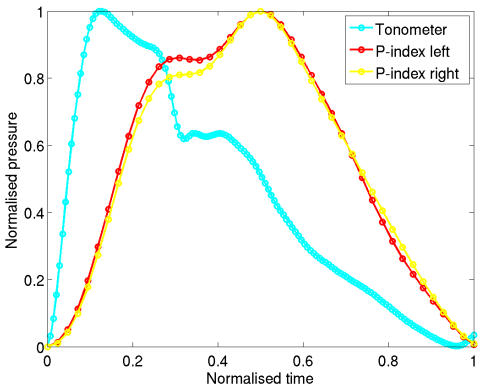

(d) YH4

Figure 16: Young healthy subjects: curves of the blood pressure measured by tonometry or deduced from the images based on the P-index (left and right hand sides). Note that the time and the pressure are normalised.

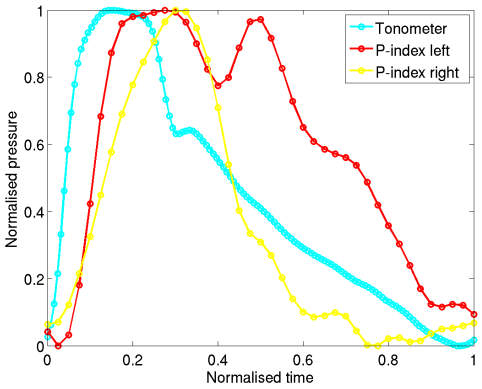

(a) MAH1

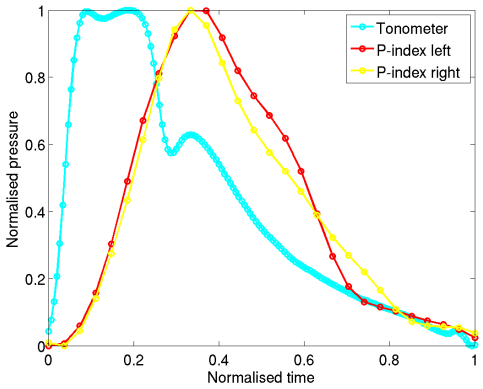

(b) MAH2

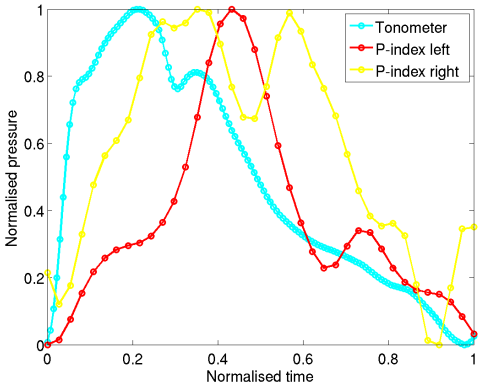

(c) MAH3

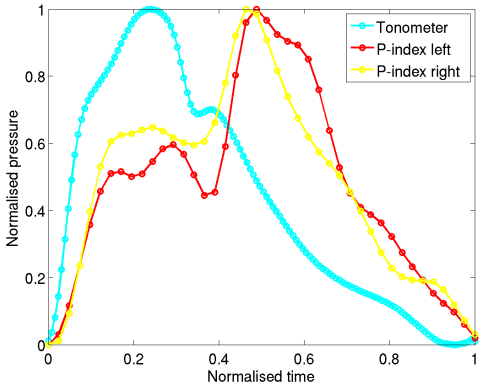

(d) MAH4

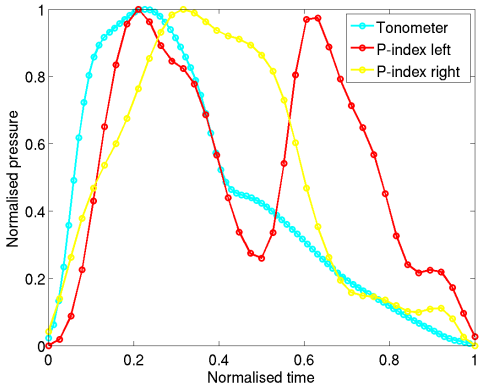

(e) MAH5

Figure 17: Mid-age healthy subjects: curves of the blood pressure measured by tonometry or deduced from the images based on the P-index (left and right hand sides). Note that the time and the pressure are normalised.

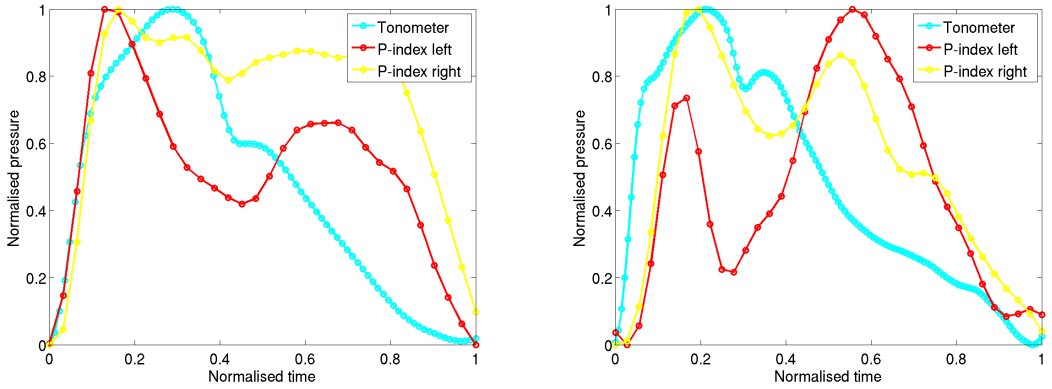

(a) OD1 (b) OD2

(c) OD3 (d) OD4

Figure 18: Old patients: curves of the blood pressure measured by tonometry or deduced from the images based on the P-index (left and right hand sides). Note that the time and the pressure are normalised.